A constitutive law for the mechanical behavior of Zr 702α

H. Francillette [a,*], A. Gavrus [b], R.A. Lebensohn [c]

[a] *GRCM, INSA, 20 Avenue des Buttes de Coësmes, 35043 Rennes Cedex, France*
[b] *MA2G, INSA, 20 Avenue des Buttes de Coësmes, 35043 Rennes Cedex, France*
[c] *IFIR, UNR-CONICET, 27 de febrero, 210 Bis Rosario, Argentina*

Abstract

A phenomenological law is proposed for the description of the mechanical behavior of Zr 702α. The identification of the parameters of the constitutive law, from macroscopic stress–strain curves of polycrystalline samples deformed in channel die compression at room temperature, indicates a good description of experiment. The implementation of the phenomenological law into a finite element code, with a Coulomb law for a more realistic description of the experimental conditions, shows good agreements between the experimental and calculated curves, and allows to describe the evolution of stress heterogeneities and of the parameters of the identified law in the samples with the plastic deformation. Moreover, the analysis of the identified parameters, from calculations performed with a self-consistent model with the initial textures of the analyzed samples, confirms the role of the active deformations modes during plastic deformation.
© 2003 Elsevier Science B.V. All rights reserved.

Keywords: Texture; Constitutive law; Slip; Twinning

1. Introduction

The study of the correlation between the plastic deformation modes and the mechanical behavior of zirconium alloys have been the subject of many investigations [1–6]. For these hexagonal materials, different modes may be active: slip glide and/or twinning. Concerning the slip systems, prismatic glide is reported to be the main active one and first order pyramidal and basal slips are reported as the secondary slip modes [3–6]. Tensile twinning of $\{1\,0\,\bar{1}\,2\}$ type or $\{1\,1\,\bar{2}\,1\}$ type may also be active [1–3]. In order to interpret experimental macroscopic stress–strain curves from the active deformation modes, polycrystalline models such as the Taylor [7], the static [8] or self-consistent [9–11] models may be used. Another way of predicting or simulating the mechanical response of materials is to use an approach based on the identification of phenomenological laws through the calculation of phenomenological parameters [12]. The aim of the present work is: (i) to determine a constitutive law for the description of the mechanical behavior of a zirconium alloy (Zr 702α); (ii) to analyze the identified parameters of the law through finite element calculations and a self-consistent model.

2. Presentation of the constitutive law

In the present study a phenomenological law, according to expression (1), is proposed for the description of the mechanical response of Zr 702α samples deformed in channel die compression tests:

$$\sigma = \sigma_0 + \sigma_{pl}[1 - \exp(-n\varepsilon)]^2 W + \sigma_{sat}[1 - W],$$
$$W = \exp(-r\varepsilon^s) \tag{1}$$

where σ_0, σ_{pl}, σ_{sat}, n, r and s are the parameters which depend on the initial texture of the deformed samples. σ is a macroscopic stress and ε a macroscopic strain which can be related to generalized macroscopic stress and strain tensors (respectively) as expressed below. The deformation process is considered here as a good approximation of rolling conditions. The tests were performed at room temperature on Zr 702α polycrystalline samples with a fine grain size (15–20 μm). In the channel die compression test, the samples were cut out from an initial sheet and recovered 3 h at 450 °C. The initial sheet presents a strong concentration of $\langle c \rangle$ axes along its normal direction (see its $\{0\,0\,0\,2\}$ pole figure and the $\varphi_1 = 0$ section of the orientation distribution function (ODF) in the Euler space in Fig. 1) [13]. By considering the different possible orientations of the samples in the channel die device, three initial textures, named ND,

* Corresponding author.
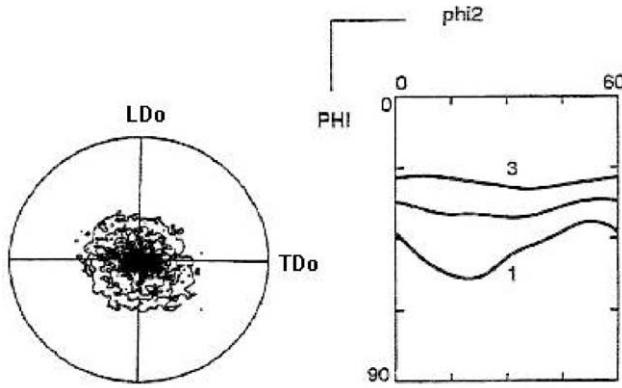
Fig. 1. $\{0\,0\,0\,2\}$ pole figure (Max $= 8.90$; levels 1–8) and $\varphi_1 = 0$ section of the initial sheet (harmonic method, crystal axes (C_1, C_2 and C_3) such as $C_1 // < 1\,0\,\bar{1}\,0 >$, $C_2 // \langle 1\,1\,\bar{2}\,0 \rangle$ and $C_3 // < 0\,0\,0\,2 >$, maximum value of the ODF: 4.20).

LD and TD were defined. In the device, ND represents the normal direction, LD the longitudinal direction and TD the transverse direction. The samples are reduced along the ND direction and are lengthened along the LD direction. Any elongation along the TD direction is forbidden during the deformation process. These textures were defined such as, noting ND_0, LD_0 and TD_0 the initial normal, longitudinal and transverse directions of the initial sheet respectively, we have:

ND texture :	$ND//ND_0$	$LD//LD_0$	$TD//TD_0$
LD texture :	$ND//LD_0$	$LD//ND_0$	$TD//TD_0$
TD texture :	$ND//TD_0$	$LD//LD_0$	$TD//ND_0$

The initial geometry was such as $h_0 = 8.6\,\text{mm}$, $L_0 = 11\,\text{mm}$ and $l_0 = 6\,\text{mm}$, h_0, L_0 and l_0 being the initial height, length and width of the samples. All the samples were deformed at an initial deformation strain rate of $9 \times 10^{-5}\,\text{s}^{-1}$. The deformation rate ε is defined by $\varepsilon = |\ln(h/h_0)|$, where h is the height of the sample under the applied stress. The true stress–strain curves (σ, ε) were determined for the different textures. Here σ and ε represent the NN components of the macroscopic stress and macroscopic deformation tensors, respectively.

In relation (1), σ_0 is a reference stress, $\sigma_{pl}[1-\exp(-n\varepsilon)]^2$ a stress contribution due to plastic deformation in the material and σ_{sat} a saturating stress value. The W term can be interpreted as a volume fraction of the material associated to the plastic deformation in the material and $(1 - W)$ can be interpreted as the complementary volume fraction associated to the σ_{sat} stress value. W equals to 1 at the beginning of the deformation process and always remains lower than this value. Eq. (1) corresponds therefore to a phenomenological mixture law with two main contributions in the polycrystalline material: the W volume fraction and its complementary volume fraction $(1 - W)$. This type of law of mixture has already been used by several authors [14–19].

It is important to note that for the establishment of a constitutive law for the analyzed textures, as a first approach, one can consider the Von Mises equivalent stress $\bar{\sigma} = (\sqrt{3}/2)\sigma$ and the generalized deformation $\bar{\varepsilon} = (2/\sqrt{3})\varepsilon$. These relations are obtained by assuming an isotropic hardening during plastic deformation in the channel die device and can then be used in a finite element code (see Section 4). A validation of the constitutive law for the different initial textures (ND, LD and TD) and for the analysis of the possible distribution of the identified parameters is possible.

3. Calculation of the parameters—experimental and calculated stress–strain curves

In the present work, the phenomenological parameters σ_0, σ_{pl}, σ_{sat}, n, s and r were calculated from the experimental stress–strain curves by an inverse analysis method. This approach as already been used by Pilvin [12] and other authors [20–22] for the identification and the characterization of the mechanical behavior of materials under various loadings (tension, compression, torsion, etc.). The calculations are performed in the present work with the OPTPAR code [20]. For a set of experimental points formally represented by a vector with p components M^{exp} and a set of calculated points noted M^{cal} (vector with p components associated with M^{exp}, determined from a given model), the relative error E_r between the predictions of the calculations and experiment can be defined by:

$$E_r = \frac{\sum_{i=1}^{p}[M_i^{exp} - M_i^{cal}]^2}{\sum_{i=1}^{p}[M_i^{exp}]^2} \tag{2}$$

where the summation is performed over the experimental data points. This term is calculated for each initial texture.

The comparison between the experimental stress–strain curves of ND, LD and TD textures and the predicted ones, from the calculated parameters according to (1), can be seen in Fig. 2. One can notice a good agreement between the predictions (dotted lines) and experiment (full lines). The values associated to these calculations are presented in Table 1. This table also indicates the relative errors E_r for all the samples. Values of E_r lower than 1% are always determined.

The anisotropy of the mechanical response of the analyzed zirconium alloy is characterized by the variety of the values of the calculated parameters. The direct interpretation of these parameters is not obvious since they appear in a quite complex expression of σ versus ε. Table 1 shows that the n parameter, and consequently the $[1 - \exp(-n\varepsilon)]^2$ term (noted F), has a little influence on the stress response of the samples when plastic deformation increases since F tends rapidly to 1 for the calculated n values. The evolution of F versus the deformation ε is shown in Fig. 3. For the main part of the curves ($\varepsilon > 0.1$) F is practically equal to 1. Then, the following relation (3) gives a good description of the macroscopic stress–strain curves with increasing plastic deformation for the calculated σ_0, σ_{pl}, σ_{sat}, r and s parameters:
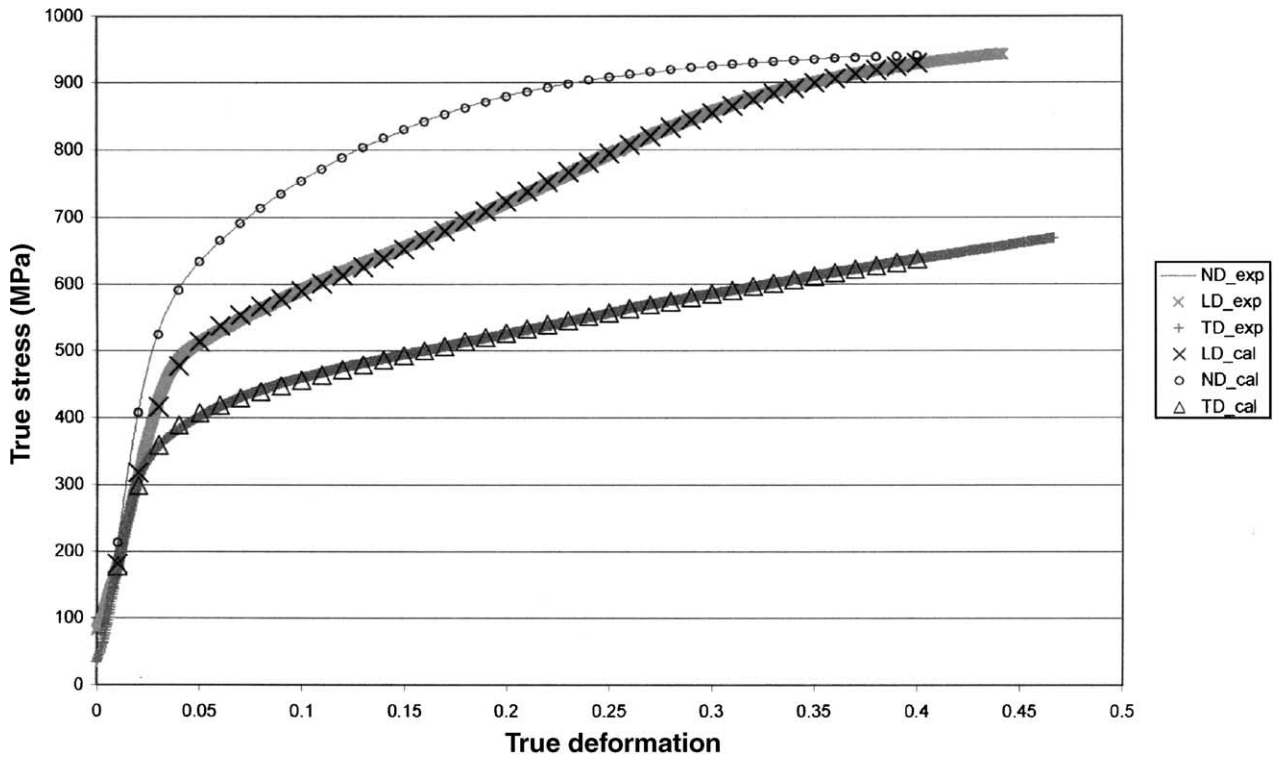
Fig. 2. Experimental (full lines) and the calculated (doted lines) true stress–strain curves for the ND, LD and TD textures; channel die compression tests.
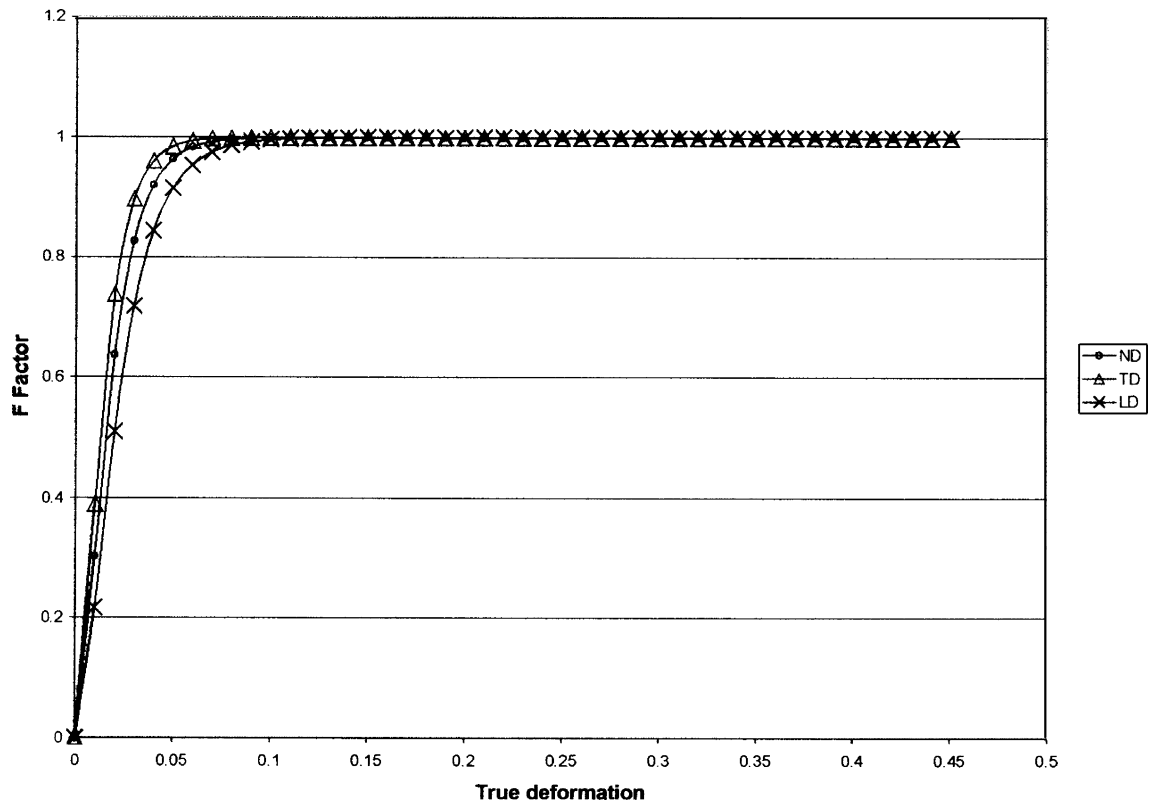
Fig. 3. Evolution of the $F = [1 - \exp(-n\varepsilon)]^2$ factor with the plastic deformation rate ε for ND, LD and TD.

Table 1
Identified parameters of the phenomenological law for the ND, LD and TD initial textures

	ND	LD	TD
σ_0	27	81	34
σ_{pl}	505.651	458.793	310.099
σ_{sat}	919.268	882.282	1533.265
n	79.886	62.6831	97.827
r	13.418	17.990	0.549
s	1.243	2.144	0.759
Error, E_r (%)	0.24	0.60	0.51

$$\sigma = \sigma_0 + \sigma_{sat} - (\sigma_{sat} - \sigma_{pl}) \exp(-r\varepsilon^s) \qquad (3)$$

It is important to note that this relation corresponds to the expression proposed by Hockett and Sherby [18] and Lloyd and Kenny [19] for aluminum, α-uranium and α-iron alloys deformed at room temperature in tension. The authors proposed this phenomenological relation (for which ε^s appears) in order to generalize the phenomenological law proposed by Voce [23] (for which only ε^s appears).

4. Analysis and discussion

In this section the interpretation of the good correlation between the experimental and predicted stress–strain curves is carried out by: (i) the introduction of the identified parameters in a finite element code in order to characterize stress heterogeneities and the distribution of the W parameter in the analyzed samples; (ii) the analysis of the active deformation modes in the different samples in order to interpret the W term in expression (1).

4.1. Implementation of the constitutive law in a finite element code

In order to validate the constitutive behavior identified by an analytical analysis of the plane compression tests for various textures, finite element simulations were carried out for each texture. In a first approach, an isotropic finite element code (the FORGE2® software) was used. The numerical simulations were considered for the three different specified textures using the Von Mises equivalent stress for the description of the behavior law as described in Section 2. As a first step, the following expression was chosen for the stress tensor $\boldsymbol{\sigma}$ for the calculations of the Von Mises equivalent stress:

$$\boldsymbol{\sigma} = \begin{array}{ccc} \text{LD} & \text{TD} & \text{ND} \\ \begin{bmatrix} 0 & 0 & 0 \\ 0 & -\frac{1}{2}\sigma & 0 \\ 0 & 0 & -\sigma \end{bmatrix} \end{array}$$

where σ is given with (1). A very small friction described by the use of the Coulomb law, with a friction constant $\mu = 0.05$, is considered in the present work between the tools and

the samples in order to have a more realistic description of the experimental conditions (use of a Teflon lubricant). The variation of the compression force along ND which depends on the specimen height is compared with the experimental curves (Fig. 4). It can be seen that a good agreement is obtained between the numerical finite element computation and the experiment. These results allows to confirm the pertinence of the proposed analytical model and the accuracy of the identification procedure.

On the other hand, the finite element calculations of Figs. 5 and 6 show the distribution of the Von Mises equivalent stress $\bar{\sigma}$ (Fig. 5) and the distribution of the W parameter (Fig. 6) for ND, LD and TD at $\varepsilon = 40\%$. For $\bar{\sigma}$ and W, the same maximum levels are used for comparing the three initial textures. Stress heterogeneities are very important in ND: there are maximum stress values at $\pm 45°$ from ND in the (ND, LD) plane. The lower stresses are obtained for TD, an intermediate situation is observed for LD. Concerning W, the repartition is quite uniform in TD, very heterogeneous in ND for which large differences are obtained. Again, an intermediate situation is obtained for LD.

It appears then that the use of Eq. (1) allows a good description of the experimental stress–strain curves. Moreover the W parameter associated to plastic deformation in the samples presents characteristic evolution for ND, LD and TD. If one considers in expression (1) that $(1 - W)$ represents the volume fraction of the material associated with the saturating stress value σ_{sat}, the W parameter can then represent the activities of the deformation modes in the samples. W can then measure the easiness of dislocation glide on slip systems or the activation of twinning. The evolution of W with plastic deformation is presented in Fig. 7 for ND, LD and TD. According to this figure, the W fraction is relatively important for the TD texture: the W volume fraction is greater than 0.8 until a plastic deformation rate of 30% and remains greater than 0.75 until 40%. But for the ND texture the W fraction decreases rapidly: at 25% plastic deformation the W fraction is lower than 0.2, and tends then to 0, when ε tends to 40%. The LD texture presents an intermediate behavior: the volume fractions remain always greater than the volume fractions of the ND texture and lower than the fractions of the TD texture with increasing plastic deformation. The plastic deformation is relatively easy for the TD texture.

4.2. Characterization of the deformation modes with a self-consistent model

For a more accurate analysis of the activities of the deformation modes, the self-consistent model developed by Lebensohn and Tomé [11] is used in this section. A complete description of the model has already been presented in previous works [10,11].

In the model the interaction law between a grain and its surrounding (homogeneous equivalent medium) is given by:

$$\dot{\boldsymbol{\epsilon}} - \dot{\mathbf{E}} = -\mathbf{M}^*(\boldsymbol{\sigma} - \boldsymbol{\Sigma}) \qquad (4)$$
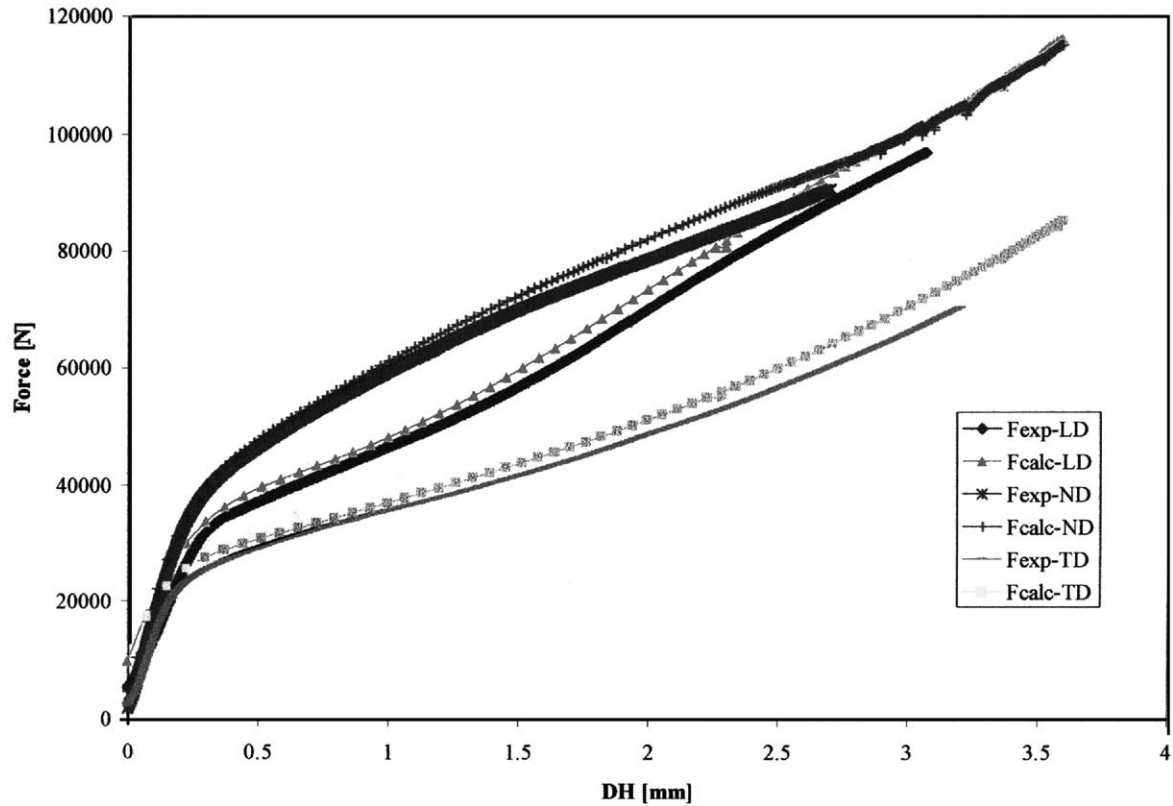
Fig. 4. Recalculated and experimental strength–displacement curves; finite element calculations assuming a Von Mises description of the behaviour law and a very small friction between the tools and the specimen—according to the use of a Teflon lubricant in the interface—described by a Coulomb law ($\mu = 0.05$).
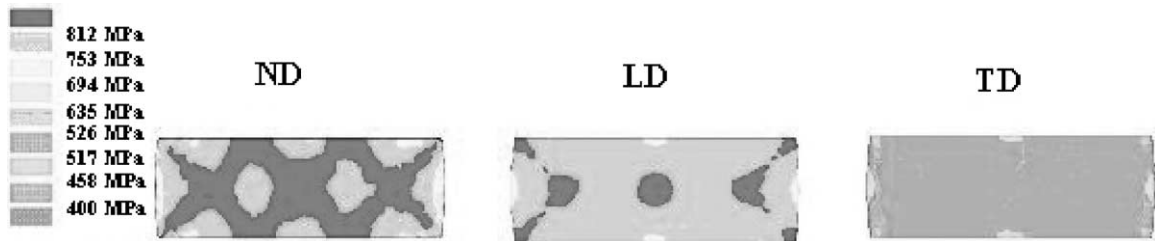
Fig. 5. Distribution of the Von Mises equivalent stress $\bar{\sigma}$ at $\varepsilon = 40\%$ in the (ND, LD) plane, finite element calculations from the identified parameters.

where $\dot{\boldsymbol{\epsilon}}$ is the strain rate tensor, $\boldsymbol{\sigma}$ the Cauchy stress tensor at the grain scale and, $\dot{\mathbf{E}}$ and $\boldsymbol{\Sigma}$ the same quantities at the macroscopic level, respectively. $\mathbf{M}^*$ is the interaction tensor determined from calculations over the polycrystal [10,11]. In the present work, the following macroscopic strain rate tensor is chosen:

$$\dot{\mathbf{E}} = \begin{array}{ccc} \text{LD} & \text{TD} & \text{ND} \\ \begin{bmatrix} 1 & 0 & 0 \\ 0 & 0 & 0 \\ 0 & 0 & -1 \end{bmatrix} \end{array} \tag{5}$$
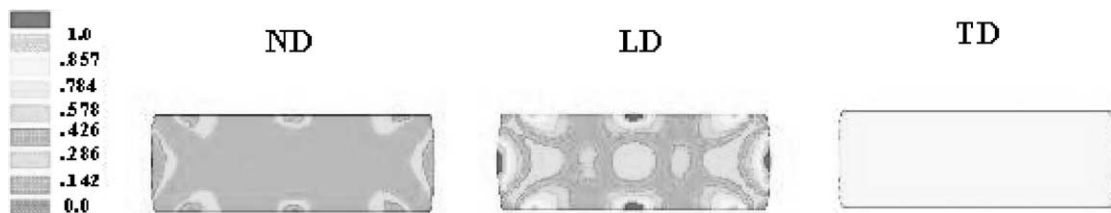
Fig. 6. W volume fraction at $\varepsilon = 40\%$ in the (ND, LD) plane, finite element calculations from the identified parameters.
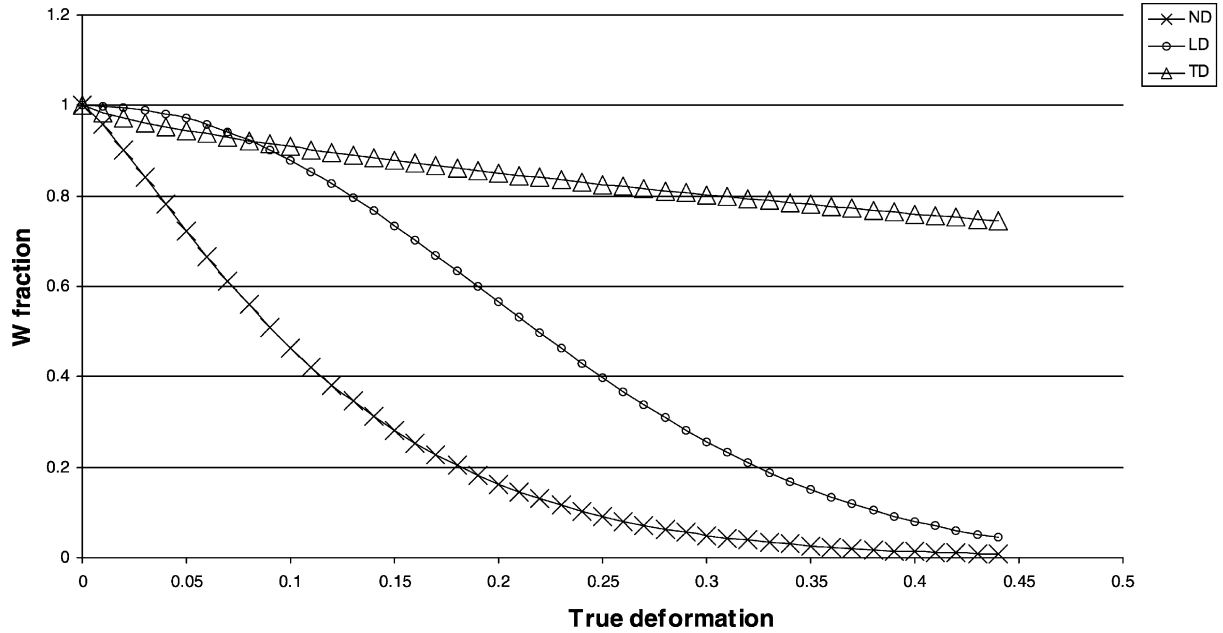
Fig. 7. Evolution of the W volume fraction with plastic deformation rate ε for ND, LD and TD textures.

The shear rate $\dot{\gamma}^s$ on a system (s) is defined by $\dot{\gamma}^s = \dot{\gamma}_0^s |\tau^s/\tau_c^s|^{n-1}(\tau^s/\tau_c^s)$, where $\dot{\gamma}_0^s$ is a normalization factor, τ^s the resolved shear stress on the (s) system and τ_c^s the reference resolved shear stress on this system ($n = 17$ in the present work). The relative activity of a deformation mode (k), noted $a(k)$ is defined by

$$a(k) = \frac{\sum_i f_i \left(\sum_{k'} |\dot{\gamma}^{k',i}| \right)}{\sum_i f_i \left(\sum_s |\dot{\gamma}^{s,i}| \right)} \qquad (6)$$

where f_i is the volume fraction associated with the (i) orientation, and $\dot{\gamma}^{k',i}$ the strain rate of the k' system of type k associated with the (i) orientation, and $\dot{\gamma}^{s,i}$ the same quantity for any (s) system. The deformation modes retained for the calculations are prismatic glide (noted P), first order pyramidal glide with $\langle a \rangle$ and $\langle c + a \rangle$ Burgers vectors (noted Pyr$\langle a \rangle$ and $\langle c+a \rangle$), basal glide noted (B) and $\{1\,0\,\bar{1}\,2\}$ tensile twinning (noted $\{1\,0\,\bar{1}\,2\}$). The following reference resolved shear stresses have been chosen for this material: $\tau_c(\mathrm{P}) = 1$; $\tau_c(\mathrm{Pyr}\langle a \rangle) = \tau_c(\mathrm{Pyr}\langle c+a \rangle) = 2.5$; $\tau_c(\mathrm{B}) = 2.5$; $\tau_c(\{1\,0\,\bar{1}\,2\}) = 1.2$. The average activities of the deformation modes are presented in Fig. 8 as a function of plastic strain.

The calculated average activities are very different for the three initial textures. Prismatic glide is the most active mode in TD: the average activity is greater than 0.9 up to 40% plastic deformation. This mechanism alone accommodates most of the plastic deformation. For the ND texture, there is a low activity of tensile twinning (average activity lower than 0.05) and there is an important activity of basal and pyramidal slips (activities near 0.4 up to 40% plastic deformation). The LD texture is an intermediate case: the activation of prismatic glide and $\{1\,0\,\bar{1}\,2\}$ twinning,

the mechanisms with the lowest reference resolved shear stresses are important. For the LD texture, the activity of $\{1\,0\,\bar{1}\,2\}$ twinning is important at the beginning of the deformation (activity greater than 0.7 at 2.5% deformation) and decreases rapidly towards 0 (it is lower than 0.1 at 25% plastic strain and lower than 3% at 40% plastic strain). First order pyramidal slip becomes more important with increasing plastic deformation: the average activity is greater than 0.4 after 20% of deformation. The activity of basal slip increases also with deformation (activity near 0.2 at 40%). These activities are correlated with the decrease of the activity of twinning with deformation. Activation of prismatic glide remains important in LD sample during all the deformation process.

4.3. Discussion

The good correlation between: (i) the experimental and predicted stress–strain curves; (ii) the evolution of the W parameter for the ND, TD and LD textures indicates that the proposed law for the material gives a satisfying link between the stress–strain curves and the plastic deformation modes of the samples. The stress levels differences observed experimentally for the different samples can be well understood by the consideration of the "soft" mechanisms of the material, namely prismatic glide and $\{1\,0\,\bar{1}\,2\}$ tensile twinning which are quite easy to activate during plastic deformation [1–6,13,24,25]. For the TD texture the $\{0\,0\,0\,2\}$ poles are in the vicinity of the transverse direction. This particular orientation of the hexagonal cells of the grains allow the reduction and the elongation of the grains by an important activation of prismatic glide. Then this result can explain the relative

important *W* fraction obtained for the TD texture for which the lowest stress levels are measured. On the other hand, the calculations with the self-consistent viscoplastic model indicate an important activation of {1 0 $\bar{1}$ 2} tensile twinning

for the LD texture. This result is consistent with the initial position of the hexagonal cells in the channel die device. For this texture the activation of prismatic glide and twinning is important but prismatic glide is less active than in the TD

(a)

(b)
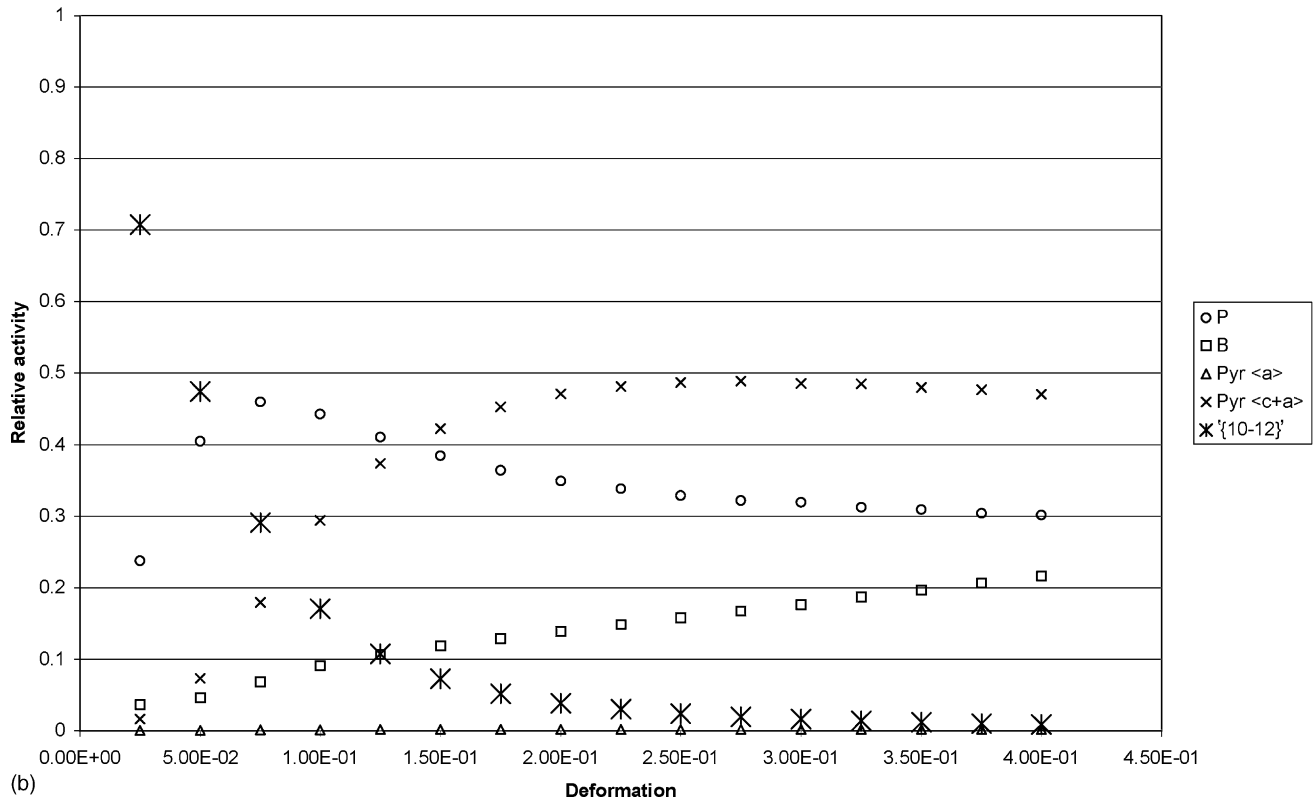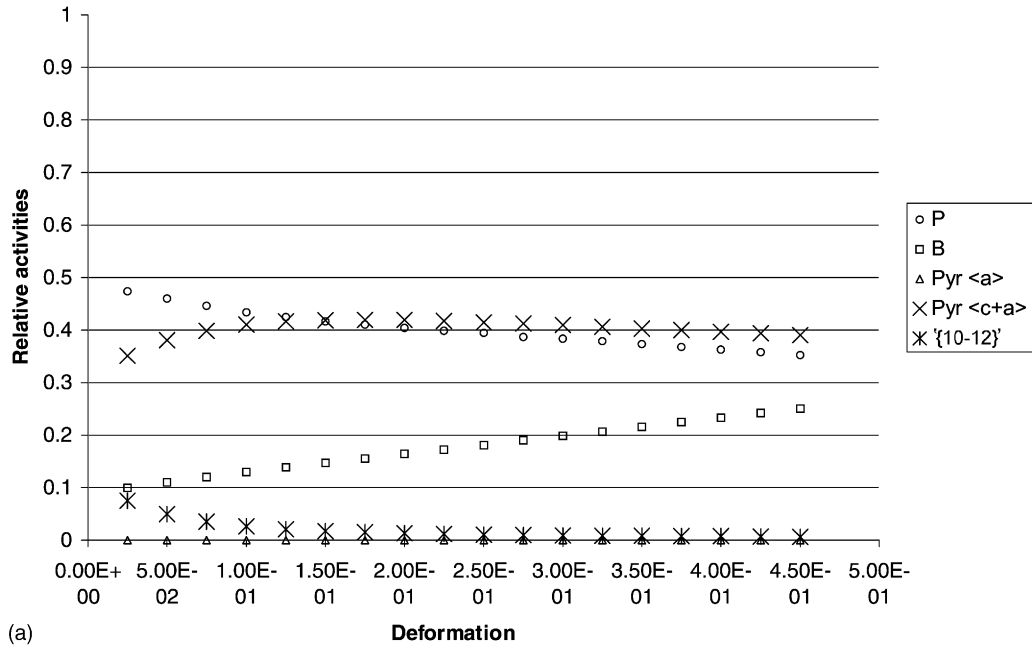
Fig. 8. Calculated activities of deformation modes; viscoplastic self-consistent model; $\tau_c(P) = 1$, $\tau_c(\text{Pyr}\langle a \rangle) = \tau_c(\text{Pyr}\langle c + a \rangle) = 2.5$, $\tau_c(B) = 2.5$, $\tau_c(\{1 0 \bar{1} 2\}) = 1.2$: (a) ND texture, (b) LD texture, (c) TD texture, (d) cumulated twinned volume fractions for ND, LD, TD.

(c)

(d)
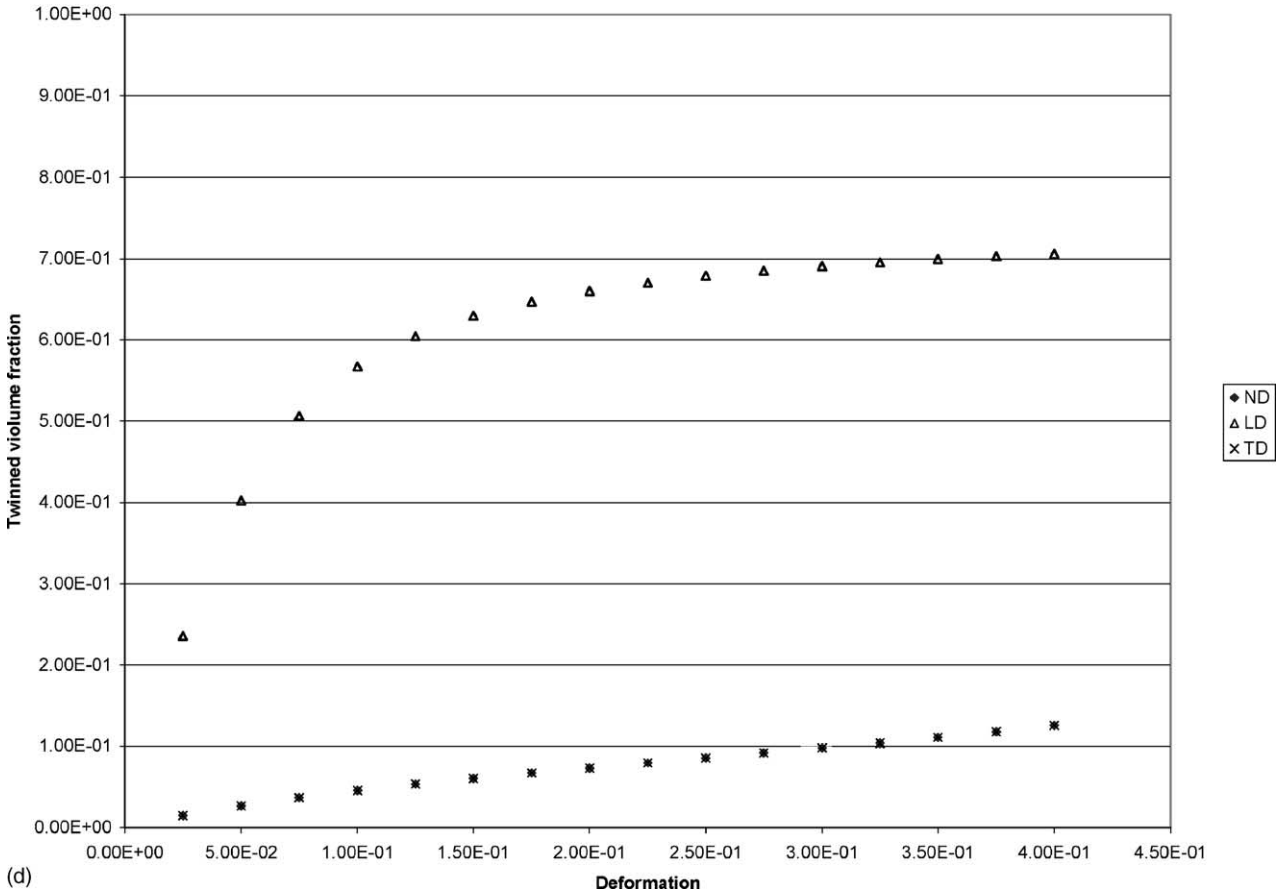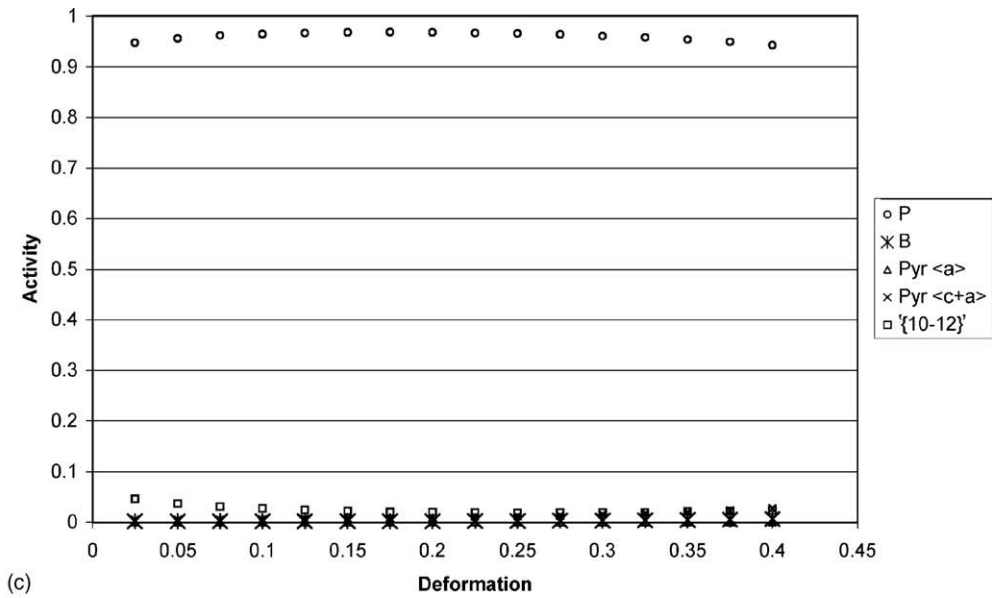
Fig. 8. (*Continued*).

texture. This result can explain the lower *W* fractions obtained for the LD texture compared to the TD texture. For ND, activation of prismatic glide and $\{1\,0\,\bar{1}\,2\}$ tensile twinning is more difficult since the hexagonal cells are initially not favorably oriented for these mechanisms. Then, pyramidal slip (with $\langle a \rangle$ or $\langle c + a \rangle$ component) is most active. This activation can explain the relative strong stress levels determined for the ND texture. Experimentally, the activation of prismatic glide is more difficult in this sample with increasing plastic deformation (strain hardening). This can

give an explanation of the saturating shape of the macroscopic stress–strain curve obtained for ND. This result can also give a satisfactory explanation of the evolution of the *W* parameter in the sample. *W* decreases rapidly towards 0 for the ND texture with increasing the plastic deformation.

5. Conclusion

A constitutive law has been proposed and identified in the present study from the macroscopic stress–strain curves of different Zr 702α polycrystalline samples (ND, LD and TD) with different initial crystallographic textures. The parameters of the law have been calculated for each initial texture and a good correlation between the experimental and the calculated curves has been found. Moreover good agreements between experimental and calculated curves were obtained using a finite element code. For an accurate interpretation of the identified coefficients, a *W* parameter associated to the plastic deformation in the samples has been drawn versus plastic deformation. This parameter indicates a quite important activation of the deformation modes in the TD texture compared to the LD and ND textures with increasing plastic deformation. For the ND texture, the *W* parameter tends to 0 and the average macroscopic stress tends to the saturating value near 40% plastic deformation. An important activation of prismatic glide is predicted for the TD texture compared to the LD and ND textures. An intermediate behavior of the *W* parameter is observed for the LD texture (values between those of TD and ND are obtained). These results can be well understood by the relative importance of the activities of $\{1\,0\,\bar{1}\,2\}$ tensile twinning and prismatic glide. It can be concluded that the interpretation of the identified parameters is consistent with the finite element calculations and the average activities of the deformation modes calculated with the viscoplastic self-consistent model.

References

[1] R.G. Ballinger, G.E. Lucas, R.M. Pelloux, The effect of plastic strain on the evolution of crystallographic texture of zircaloy-2, J. Nucl. Mater. 126 (1984) 53–69.

[2] P. Robinet, Etude expérimentale et modélisation du comportement viscoplastique anisotrope du zircaloy-4 dans deux états métallurgiques, Doctorate Thesis, University of Franche-comté, France, 1995.

[3] A. Akhtar, A. Teghtsoonian, Plastic deformation of zirconium single crystal, Acta Metall. 19 (1971) 655–663.

[4] H. Numakura, Y. Minonushi, M. Koiwa, $\langle \bar{1}\,\bar{1}\,2\,3 \rangle \{1\,0\,\bar{1}\,1\}$ slip in zirconium, Philos. Mag. A 63 (5) (1991) 1077–1084.

[5] P. Merle, Evidence of pyramidal slip mode in cold-rolled zircaloy-4 sheets, J. Nucl. Mater. 144 (1987) 275–277.

[6] A. Akhtar, Basal slip in zirconium, Acta Metall. 21 (1973) 1–11.

[7] G.I. Taylor, Plastic strains in metals, J. Inst. Met. 62 (1938) 307.

[8] A. Molinari, L.S. Tòth, Tuning a self consistent viscoplastic model by finite element results. I. Modeling, Acta Metall. 42 (1994) 2453–2458.

[9] L.S. Tòth, A. Molinari, Tuning a self consistent viscoplastic model by finite element results. II. Application to torsion textures, Acta Metall. 42 (1994) 2459–2466.

[10] R.A. Lebensohn, Deformacion plastica de metals policristalinos. Modelizacion del desarollo de textura asociado al trabajo mecanico, Doctorate Thesis, Instituto de fisica Rosario, UNR-CONICET, Argentina, 1993.

[11] R.A. Lebenshon, C.N. Tomé, A self-consistent approach for the simulation of plastic deformation and texture development of polycrystals: application to zirconium alloys, Acta Mater. 41 (1993) 2611–2624.

[12] P. Pilvin, Multiscale approaches for the description of the inelastic behaviour of metallic materials, Doctorate Thesis, University Paris 6, France, 1990.

[13] H. Francillette, B. Bacroix, M. Gaspérini, J.-L. Béchade, Grain orientation effects in Zr702α polycrystalline samples deformed in channel die compression tests at room temperature, Acta Metall. 46 (1998) 4131–4142.

[14] J.-H. Schmitt, P. Fabregue, B.J. Thomas, Recristallisation dynamique dans les aciers, Journal de Physique IV, Colloque C3, supplément au Journal de Physique III 5 (1995) 153–163.

[15] M.J. Luton, C.M. Sellars, Dynamic recrystallization in nickel and nickel–iron alloys during high temperature deformation, Acta Metall. 17 (1969) 1033–1043.

[16] C.M. Sellars, in: Proceedings of the Seventh International Symposium on Metallurgy and Material Science (RISO), Roskilde, 1986, p. 167.

[17] A. Laasraoui, J. Jonas, Prediction of steel flow stresses at high temperatures and strain rates, Metall. Trans. 22A (1991) 1545–1558.

[18] J.E. Hockett, O.D. Sherby, Large strain deformation of polycrystalline metals at low homologous temperatures, J. Mech. Phys. Solids 23 (1975) 87–98.

[19] D. Lloyd, D. Kenny, The structure and property of some heavily cold worked aluminium alloys, Acta Metall. 28 (1980) 639–649.

[20] A. Gavrus, Identification automatique des paramètres rhéologiques par analyse inverse, Doctorate Thesis, Ecole Nationale Supérieure des Mines de Paris, France, 1996.

[21] D.M. Bates, D.G. Watts, Non Linear Regression Analysis and its Applications, Wiley, New York, 1988.

[22] P.E. Gil, W. Murray, M.H. Wright, Practical Optimization, Academic Press, London, 1981.

[23] E. Voce, J. Inst. Met. 74 (1948) 537.

[24] E. Tenckhoff, The development of the deformation texture in zirconium during rolling in sequential passes, Met. Trans. A 9 (1978) 1401–1412.

[25] N. Christodoulou, Evolution of the Bauschinger effect in tension and compression in zircaloy-2, Acta Metall. 37 (1989) 529–539.